Preferred citation: C.C. Habeger and G.A. Baum. Ultrasonic characterisation of fibre suspensions. In **The role of fundamental research in paper-making**, *Trans. of the VIIth Fund. Res. Symp. Cambridge, 1981*, (Fundamental Research Committee, ed.), pp 277–308, FRC, Manchester, 2018. DOI: 10.15376/frc.1981.1.277.

ULTRASONIC CHARACTERISATION OF FIBRE SUSPENSIONS

C. C. Habeger and G.A. Baum
The Institute of Paper Chemistry
Wisconsin, USA.

Abstract

This paper presents the results of an experimental and theoretical investigation into the fundamental mechanisms that govern ultrasonic propagation in fibre slurries. An experimental apparatus which measures the attenuation and velocity of ultrasound in slurries is described. Measurements on wood fibre slurries show, in contrast to previous work, that the effect of the fibre on the velocity of ultrasound is negligible. This observation led to the development of an isolated segment model, which can predict attenuation as a function of fibre properties and ultrasonic frequency. The theory assumes the fibres are isolated, isotropic, infinite cylinders. It accounts for scattering, heat conduction, viscous losses in the fluid, and relaxation processes in the fibre. Experiment and theory are shown to be in good agreement for some synthetic fibre slurries. In the more complicated case of wood fibre suspensions, the theory predicts attenuation to the correct order of magnitude and permits speculation about the effects of fibre properties.

Introduction

Non-destructive analysis of fibre slurries using ultrasonic techniques may some day be a valuable tool for determining fibre properties. Previous authors[1,2] have described how ultrasonic attenuation in a wood fibre suspension is proportional to its consistency. They have also demonstrated that the attenuation at a given consistency varies with furnish. Adams[2] reported how the attenuation is also a function of the amount of refining. Ultrasonic attenuation is thus sensitive to the origin and treatment of a wood fibre suspension. It should be possible to characterise the slurry by measuring attenuation as a function of frequency. However, progress in this area is hampered by the lack of understanding of wave propagation in fibre suspensions. In fact, from previous work, it is not even possible to identify the major loss processes.

The theoretical models of wave propagation in heterogenous fluid-solid mixtures can be classified as isolated segment models or as porous solid models. The isolated segment models calculate the loss due to a single solid element surrounded by the fluid and assume that the total loss is the sum of the effects of the individual elements. Interactions between solid elements are not considered. An example of this, for cylindrical segments, is the Rayleigh-Sewell model[(3)]. In this, losses from scattering and viscous processes caused by the presence of rigid, immovable cylindrical inclusions in a viscous fluid are calculated. The Rayleigh-Sewell model predicts that the slope of the curve of $\ln(a/f^2)$ vs. $\ln(f)$ should always increase with f (a is the attenuation coefficient and f is the frequency). This is contrary to the results of the experiments on wood fibre suspensions described by McFarlane and Llewellyn[(1)], and by Adams[(2)]. A more complete isolated segment model is that of Allegra and Hawley[(4)]. It allows for shear and normal strains in the solid, considers thermodynamic effects, and accounts for relaxation processes in the solid. The Allegra-Hawley theory predicts the attenuation vs. frequency behaviour of polystyrene spheres in water from independently determined bulk properties of polystyrene[(4)]. Curiously, in the ranges of frequencies and radii studied, energy dissipation due to heat conduction in the solid-boundary region is the dominant loss process. Sadly, the Allegra-Hawley model is developed only for spherical segments and is not applicable to fibre suspensions.

In the porous solid models, the solid fraction is assumed to form a porous structure, and the mechanical properties of the structure are important. The Biot model[(5)] is a well-developed porous solid theory which assumes that the fluid is contained in parallel cylindrical capillaries and that the attenuation arises from viscous flow within them. It is possible to include the effects of solid relaxation processes, but scattering and thermal loss processes are ignored. An additional drawback of the Biot theory is the difficulty of estimating model parameters. It is hard enough to obtain the bulk fibre properties needed by the isolated solid theories, but discovering the mechanical parameters for the structures and the interaction parameters between structure and fluid needed by the Biot model is far more difficult.

If frequency-dependent velocity changes existed and could be measured along with attenuation, there would be additional information available for slurry characterisation. This was the path taken by Adams[2], who measured velocity and attenuation. He reported that wood fibres do cause a frequency-dependent velocity shift. Since porous solid models predict a frequency-dependent velocity shift, while isolated segment models do not, Adams made use of the Biot model to explain his results. He also obtained data indicating that attenuation is not linear when different fractions of two different pulps are mixed. This is contrary to the predictions of the isolated segment models. In contrast, McFarlane and Llewellyn[1] and Adams[2] found that attenuation is linear with solid fraction, an observation more in line with the predictions of the isolated segment models than with those of the porous solid models. Adams did not attempt to predict his experimental results from independent determinations of the Biot parameters: but he did show that Biot parameters do exist which give the observed shape of the velocity and attenuation curves.

Experimental

The apparatus we constructed to measure ultrasound velocity and attenuation in fibre slurries is a pulsed radio frequency (rf) interferometer designed to operate over a range from 0.6 to 13 MHz: this was similar to Adams′ design.

A schematic diagram of the apparatus is shown in figure 1. The rf signal from a stable continuous wave (CW) source is mixed with a pulse to produce a pulsed rf signal. This is applied to a piezoelectric transmitter which is immersed in the suspension. An identical transducer receives the signal after it has passed through a length, L, of fibre suspension. The signal received is attenuated to a standard level, amplified, and mixed with the continuous wave.

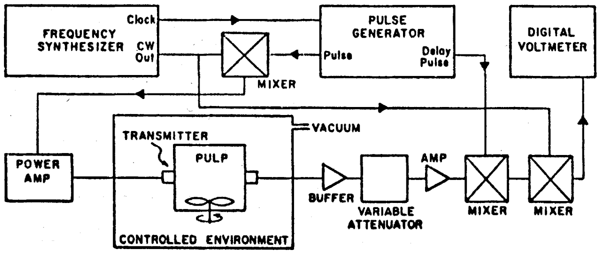

Fig 1—Schematic diagram of the apparatus for the ultrasonic characterization of fibre suspensions.

The phase of the received signal depends on the phase shift in the suspension, $2\pi Lf/V$, where f represents the frequency of the CW signal and V is the velocity of ultrasound in the suspension, plus the phase shift in the transducers. The mixed signal amplitude reaches a maximum when the phase difference between the CW signal and the received signal is an integral multiple of 2π. As frequency changes, the phase of the received signal progresses and the mixed output oscillates. The velocity of sound in the suspension can be calculated from the frequency difference between minima in the mixed output, provided the phase shifts outside the suspension can be accounted for. The degree of attenuation in the suspension can be determined from the value of attenuation of the CW signal necessary to produce the standard signal level.

In order to obtain very accurate velocity measurements, our apparatus differed from Adams′ in two ways. The CW signal source is not an oscillator, but a frequency synthesizer stable to one part in 10^7. This gives a resolution of one part in 10^5 in the frequency shift measurements in homogeneous fluids. In addition, the transducers are mounted so that their separation distance can be varied. This allows the frequency-dependent phase shifts in the transducers to be measured, thus allowing correction of the velocity data. Adams estimated these shifts from a mathematical model of the transducers.

The suspension is contained in a plexiglass tank 0.5m long, 0.2m wide and 0.2m high (see figure 2). Four transducer pairs are mounted in a frame and suspended above the slurry on precision screws.

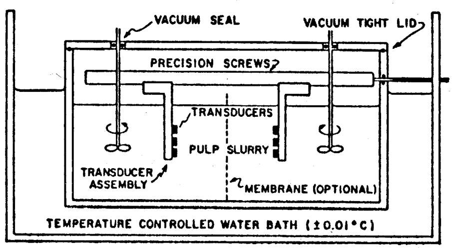

Fig 2—Simplified cross section of sample chamber.

This allows the transducer separations to be varied. The four transducer pairs are necessary to cover the frequency range from 0.6 MHz to 13 MHz. The entire assembly is immersed in a water bath whose temperature is controlled to within 0.01°C. The suspension is mixed by a pair of stirrers mounted behind the transducer assemblies and rotating in opposite directions.

A second technique can be used for measuring the ultrasound velocity. The sample chamber can be separated into two parts by inserting a 0.006mm thick Mylar membrane between the transducer assemblies. By placing water in one compartment and the fibre suspension in the other, the velocity can be measured by a second technique. The transducer assemblies are moved along the supporting screws with their separation fixed, thus changing the relative amounts of water and fibre seen by the transducer pairs. The velocity is then calculated from the change in distance necessary to move the mixed output signal between minima.

Velocity measurements

Equation (1) gives the velocity of sound, V, in the fluid, accounting for the frequency-dependent phase shifts in the transducers.

$$V = \frac{L\Delta f}{1 - \frac{d\varphi\Delta f}{df2}} \tag{1}$$

Here L is the transducer separation, Δf is the frequency difference between minima in the mixed signal output, and $d\varphi/df$ is the derivative of the transducer phase shift with respect to frequency. By making measurements at two transducer separations and setting the resulting left hand side of Equation (1) equal, the transducer effect can be calculated.

The transducer effect in terms of the Δf's at two separations is

$$w = \frac{1}{2\pi}\frac{d\varphi}{df} = \frac{L_2\Delta f_2 - L_1\Delta f_1}{\Delta f_1\Delta f_2(L_2 - L_1)} \tag{2}$$

This approach was first tested on distilled water. Measurements of Δf were made with the four transducer pairs at three separations (50, 100 and 150 mm). The three possible values of w were calculated and averaged. The velocity was then calculated from Equation (1) for the three values of L and Δf. Figure 3 shows the results for one transducer pair (5 MHz).

The three lower solid curves represent the apparent velocities (L Δf) at each separation distance, and the top solid curve is the average corrected curve for distilled water.

At all frequencies, the corrected water values were within 0.15% of the value of the velocity in distilled water given in tables. At frequencies above 1.2 MHz, the agreement was to better than 0.07%. The system is thus able to give stable and accurate measurements of ultrasonic velocities in homogeneous fluids.

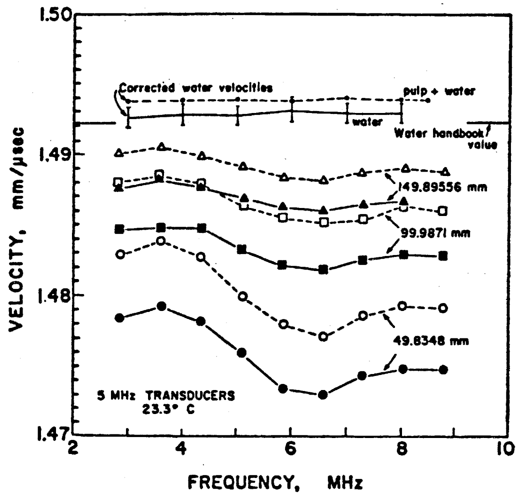

Fig 3—Apparent and corrected velocities as a function of frequency. The solid points and curves are for distilled water at transducer separations of 49.835 mm (●), 99.987 mm (■), and 149.896 mm (▲). The open points and dashed lines are for a 0.48% consistency bleached kraft pulp, at the same transducer separations. The two uppermost curves are the corrected water and slurry velocities.

The results obtained by applying the same procedure to a 0.48% consistency bleached kraft pulp beaten to 90 CSF are shown in figure 3 as dashed lines. The pulp slurry has a different mechanical impedance from pure water so that the correction for transducer phase shifts is smaller.

Over the entire 0.6 - 13 MHz range, the corrected velocity of the pulp is an average of 0.06% higher than that of water, with a standard deviation of 0.05%. So, there is a small increase in velocity, but no significant frequency dependence.

Tests were conducted on pulps of up to approximately 3% consistency. The apparent velocity was measured at the 50 mm transducer separation only, and the values of w found from the water experiments were used to calculate the corrected velocities, thus tending to overestimate the slurry velocity.

However, the largest deviation from the velocity in distilled water was only +0.6%, and again no frequency dependence was detected.

Since the effect of fibres on the velocity of ultrasound in water is a crucial question, the second velocity measurement technique was also used. This was the water-diaphragm-pulp method discussed above. A constant separation of 150mm was maintained between transducers, and the apparent velocity was measured as the transducers were moved relative to the diaphragm. As the transducers were moved, the components due to the transducer phase shifts remained constant. The only change, therefore, was in the path lengths of the ultrasound in pulp and water. These measurements were made in a 0.96% consistency slurry of 90 CSF bleached kraft pulp, and a 0.77% consistency slurry of 720 CSF bleached kraft pulp. For the pulp of 720 CSF the velocity was 0.12($\pm$0.11)% greater than for water, and for the 90 CSF pulp the velocity was 0.12($\pm$0.4)% greater than for water. This is consistent with our earlier results.

We must conclude that the velocity of ultrasound in a wood fibre suspension does not, to the first order, differ from the velocity in water, and is not frequency dependent. The above results allow us to reject the porous solid models discussed earlier and to use an isolated segment model to explain the attenuation results. Such models have parameters that are more likely to be independently determined. The Allegra-Hawley model is the only isolated segment model complete enough to handle realistically polymeric fibre suspensions, but it only applies to spherical inclusions. It was necessary, therefore, to develop an Allegra-Hawley model for infinite length cylindrical inclusions. The resulting theory, which will be published elsewhere, is outlined in the Appendix and briefly described below.

Theory

The Allegra-Hawley isolated segment model for spheres calculates the attenuation by finding exact solutions for the strain and temperature to the governing differential equations of continuity, motion, and energy conservation.

The model considers a single solid segment in a fluid medium. The solution must be a plane compressional wave far away from the inclusion and the boundary conditions of equal stress, velocity, temperature, and heat flux must be met over the solid-fluid interface. The solution is found by expanding the incoming plane wave in terms of spherical harmonics. Solutions are expressed in terms of three scalar potentials in the fluid and three in the solid. The total solution is the plane wave plus the potentials expanded in spherical harmonics with undetermined coefficients. The coefficients are found by applying the boundary conditions to each order of spherical harmonics. The result is six equations and six unknowns for each order. These are solved numerically for the zeroth, first, and second order. As long as the radius of the sphere is less than the wavelength of the compressional wave, the series converges rapidly, and the first few orders are sufficient for a practical solution. The attenuation is calculated from these coefficients.

In order to apply this model to fibres, the calculation is repeated for infinite cylindrical, isotropic inclusions. For this case the plane waves and potential functions are expanded in terms of Bessel functions and sinusoidal functions. For the spherical case, symmetry arguments show there is no velocity or stress in the φ direction. For the cylinder there are velocities and stresses in the z, r, and θ directions; therefore, there are more boundary conditions and a fourth potential is needed. In addition, the solution depends on the orientation of the incoming wave to the plane of the cylinder; thus, attenuations are found for a set of orientations and numerically integrated to get the result for randomly orientated fibres. The result of this theoretical development is a computer program that gives the attenuation as a function of frequency when the following parameters are given:

cylinder radius (R')
solid and fluid compressional wave velocity (c',c)
densities (ρ',ρ)

solid Poisson's ratio (ν')
fluid viscosity (η)
the thermal conductivities (K',K)
the thermal expansion coefficients (B',B)
the heat capacities (Cp',Cp)
temperature (T)
solid loss tangent ($\tan \delta$)
and solid volume fraction (fr).

Although the different processes interact, it is possible to make some qualitative statement about the relative importance of scattering, viscous losses, thermal losses, and solid relaxation processes. Thermal effects peak at a frequency where the skin depth of the thermal wave is of the order of the radius. For the radii of interest (1 to 100 μm) this happens below the lowest experimental frequency (0.6 MHz), and thermal processes make a significant contribution only for the thinnest fibres at the lowest frequencies. Since in most cases this means that the thermodynamic coefficients are not important, the complexity of the prediction process is reduced. Viscous drag is a maximum when the skin depth of the fluid viscous wave is of the order of the radius. This occurs at a higher frequency than for the thermal case and viscous processes make a strong contribution at the lower frequencies and radii studied. Relaxation contributes at all frequencies and can be the dominant attenuation component when the loss tangent is large and there is a good impedance match between fluid and solid. Scattering is a major factor at the higher radii and frequencies.

Limitations to the theory when applied to actual fibre suspensions result from

(1) fibre anisotropy
(2) finite fibre length
and (3) non-cylindrical fibre shapes.

Concerning item 2, a difference between finite and infinite fibres arises when the loss factor is small. Figure 4 shows theoretical plots of the relative attenuation of a single fibre as a function of e , the angle between the plane of the fibre and the incoming radiation, at different values of loss tangent. Notice the strong peak for low loss tangents. This occurs when the wave-vector of the incoming radiation, as projected along the fibre, equals the wave-vector of the zeroth order longitudinal rod mode in the cylinder. The velocity of this mode is approximately $(E'/\rho')^{1/2}$ when the wavelength of the bulk compressional wave in the solid is much greater than the radius (E' is Young's modulus of the solid and ρ' is the solid density).

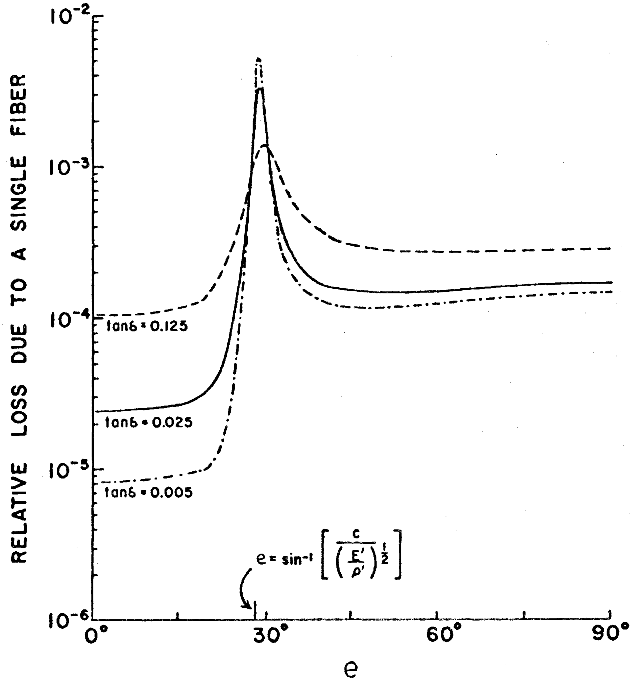

Fig 4—Theoretical plots of the relative loss per single fibre *vs.* the angle, ϵ, between the incoming radiation and the plane of the fibre. The slurry parameters are $\rho = 996$ kg/m^3; $\rho' = 1340$ kg/m^3; $\eta = 9.4 \times 10^{-4}$ nt·sec/m^2; K = 0.59 watts/m°K; K′ = 0.038 watts/m°K; c = 1490 m/sec; c′ = 4000 m/sec; $\nu' = 0.35$; Cp = 4.14×10^3 J/kg°K; Cp′ = 1.02×10^3 J/kg°K; $\beta = 2.36 \times 10^{-4}$/°K; $\beta' = 1.7 \times 10^{-5}$/°K; f = 1 MHz; T = 296°K; and R′ = 13×10^{-6} m. A list of symbols is in the appendix.

At this particular angle, for an infinite cylinder, disturbances from the incoming radiation on the cylinder interfere constructively, and large motions are excited in the cylinder. This phenomenon requires communication between distant parts of the fibre and would not be seen experimentally on short fibres. When the loss factor is high, communication over larger distances is lost, even for infinite cylinders, and the theory is more applicable. Differences between experiment and the infinite cylinder model are expected when the quantity $2\pi f.\tan \delta/c'$ is less than the inverse fibre length.

Attenuation results

Preliminary attenuation measurements on wood fibre slurries confirmed many of the results reported by Adams(2). Within experimental error, attenuation was proportional to consistency. This was also true for the synthetic fibre systems. Air bubbles had a large effect on attenuation at the lower frequencies. Slurries had larger attenuation before degassing at frequencies below about 2 MHz. Because of the air effects, slurries were routinely degassed overnight before testing. Also, as will be discussed later, refining tended to decrease the attenuation in bleached kraft pulps.

Because of problems in characterising wood pulp fibre sytems, the majority of the data presented here are from synthetic fibre suspensions. Such fibres have similar dimensions and physical properties, which is helpful in identifying those parameters most important in ultrasound attenuation. The properties of the synthetic fibres studied are included in Table 1.

The results of the experimental and theoretical attenuation studies are reported by fibre category. The data are represented, as is customary, by plots of attenuation divided by frequency squared vs. frequency. The attenuation data are divided by the consistency to normalise the curves to a 1% consistency slurry. The data come from four transducers at two separations (100mm and 150mm) and often two consistencies.

Fibre Type	Radius µm	Rod Velocity at 60 KHz km/s	Instron Modulus 10^9 N/m^2	Figures	Comment
Nylon 6,6	13-16	1.66(wet)	3.09	5	
Nylon 6	110-120	2.13(dry)	2.87	6	
Polyester	13	4.00(wet)	10.7	7,8	
Rayon	11-15	0.91(wet)		9,10	Regular Modulus
Rayon	7-10	1.27(wet)		11	Hi-wet Modulus

Table 1
Synthetic fibre properties

1. NYLON

Nylon is very hygroscopic, and water acts as an effective plasticiser. This leads to a relatively high loss tangent. For swollen nylon fibres in the frequency range studied, handbook values indicate a loss tangent value of between 0.1 and 0.2. The theoretical model predicts that thermal phenomena should not have a significant effect on the attenuation. Thermal processes would contribute if the radii were of the order of 1 µm, or if the frequencies used were two orders of magnitude smaller (10 kHz).

Figure 5 gives results for a slurry made from a 15.2±1 µm radius nylon 6,6 fibre, cut to lengths of 2.3 mm.

The model requires that the elastic properties of the fibres be known. For an isotropic solid two independent elastic parameters must be specified. The longitudinal wave velocity in a rod can be measured to fix one parameter, since this velocity equals $(E'/\rho')^{1/2}$. Using techniques developed for in-plane measurements on paper, the velocity of this mode in the saturated nylon fibres was 1.66km/s at 60 kHz. The value of Poisson's ratio was taken as the other unknown parameter, though the fibre shear modulus, μ, might equally have been used, since $\mu' = E'/2(1+\nu')$.

In figure 5, for the theoretical attenuation curve the loss tangent was set equal to 0.1, the lower handbook value. Actually the effect of loss tangent on these curves is quite small, a change from 0.05 to 0.2 causing only 10% difference in the curves. The only significant unknown parameter, therefore, is the Poisson's ratio, and this may be varied to obtain the best fit. Good agreement between experiment and theory occurs when it has the value 0.3.

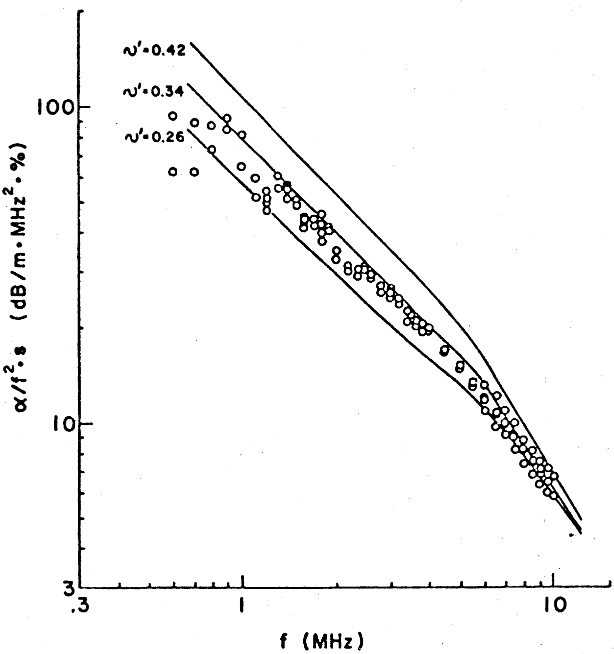

Fig 5—Experimental attenuation data for a nylon 6,6 fibre slurry with radii from 13 to 16 μm and a length of 2.3 mm. The accompanying lines are theoretical curves for different values of fibre Poisson's Ratio. Model fibre parameters are $\rho' = 1090$ kg/m^3; $V_R' = 1660$ m/sec; $K' = 0.36$ watts/m°K; $Cp' = 1.42 \times 10^3$ J/kg°K; $\beta' = 1.0 \times 10^{-5}$/°K; $\tan\delta = 0.1$; $R' = 15.2 \times 10^{-6}$ m; and s = 1.08%. For water parameters see Figure 4.

The value of $k'_c.l'.\tan\delta$ is unity at about 1.4 MHz, indicating that deviation between theory and experiment might be expected at lower frequencies due to the finite length of the fibres.

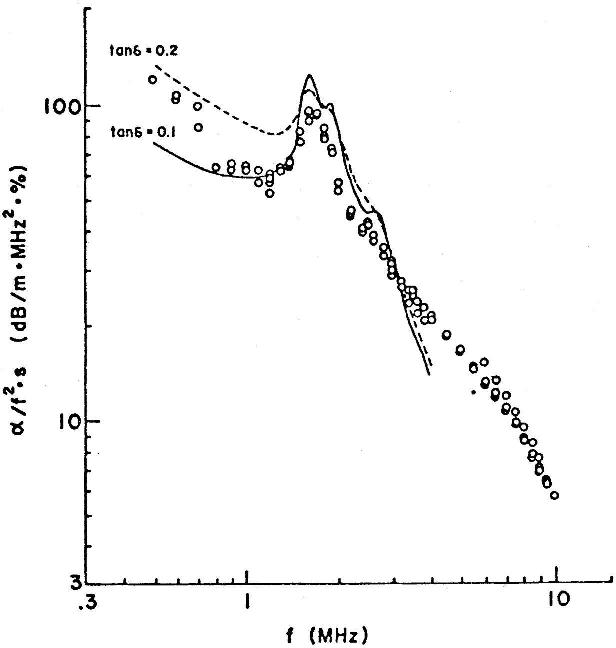

Fig 6—Experimental attenuation data for a nylon 6 fibre slurry with radii from 110 to 120 μm and a length of 2.3 mm. The theoretical lines are for different values of the loss tangent. Model fibre parameters are $\rho' = 1090$ kg/m^3 ; $c' = 1340$ m/sec; $\nu' = 0.30$; $K' = 0.36$ watts/m$^\circ$K; $Cp' = 1.42 \times 10^3$ J/kg$^\circ$K; $\beta' = 1.0 \times 10^{-5}/^\circ$K; $R' = 115 \times 10^{-6}$ m; and s = 1.08%. Figure 4 has the water parameters.

The effect of radius can be predicted by calculating theoretical curves at the same consistency, but with different radii. The results show that attenuation increases somewhat with radius, ie $d(\ln a)/d(\ln R') = 0.27$ at 1 MHz.

Figure 6 shows the results for much larger ($R'=115\pm5$ µm) nylon 6 fibres. The theoretical plots show the effects of different loss tangents. The Poisson's ratio is assumed to be 0.3 because of the good fit in figure 5. Because of difficulties in measuring ultrasound velocities in saturated fibres of this type, the longitudinal velocity was estimated by assuming that the ratio between the wet and dry state velocities is the same in this sample as in the other nylon fibres tested. The maximum in the attenuation at 1.7 MHz for both theoretical and experimental curves is due to scattering. Notice that the low loss tangent theoretical curve has three scattering peaks. These peaks become more prominent at still lower values of loss tangent. The loss tangent appears to have a significant effect at the lower frequencies but becomes inconsequential at higher frequencies once scattering dominates the attenuation.

2. POLYESTER

The attenuation data for 2.3mm long polyester fibres with 13µm radii and 4.0 km/s rod velocities are shown in figure 7. Figure 8 shows the results for the same material cut to 1.6mm lengths. The evenly spaced oscillations in the experimental data are surprising.

Unlike nylon, polyester is not hygroscopic and has a small loss tangent. The theoretical curves are insensitive to the value of the loss factor, making Poisson's ratio the only adjustable parameter. It is possible to choose a value of this such that the theory predicts the average behaviour of the experiments. The solid lines in figures 7 and 8, which approximate the data if the oscillations are ignored, have Poisson's ratio 0.4. This average fit may be fortuitous because for the 2.3 mm fibres, $k_c'.l'.\tan\delta$ has the value unity at about

17 MHz. This means that the infinite cylinder model should not be applicable over most of the frequency range.

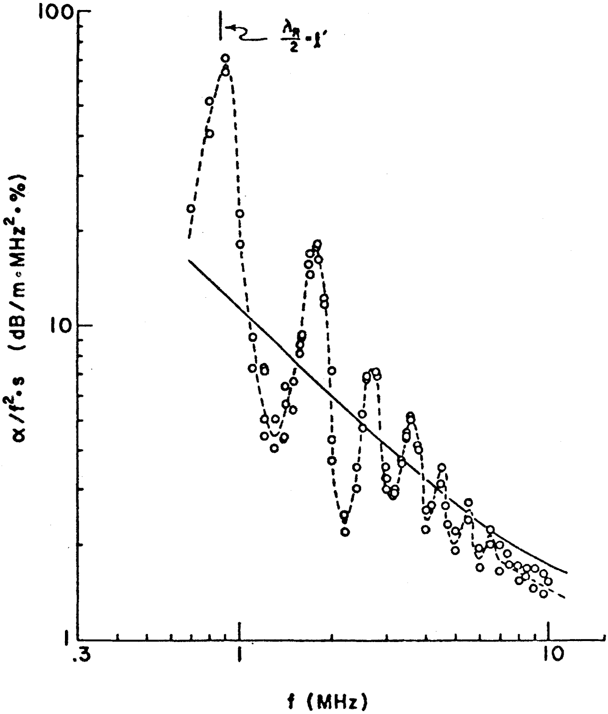

Fig 7—Experimental attenuation data for a polyester fibre slurry with a radius of 10.7 μm and a length of 2.30 mm. The model fibre parameters for the theoretical curve are $\rho' = 1340$ kg/m^3; $c' = 5860$ m/sec; $\upsilon' = 0.4$; $K' = 3.8 \times 10^{-2}$ watts/m°K; $Cp' = 1.02 \times 10^3$ J/kg°K; $\beta' = 1.7 \times 10^{-5}$/°K; $R' = 13 \times 10^{-6}$ m; and $s = 1.00\%$.

The explanation for the observed oscillations becomes clear when it is noticed that the period and phase are length dependent. The loss tangent is small and the fibres are short enough that a significant resonant vibration can occur when the fibre length is an integral number of half wavelengths of the longitudinal rod mode. The frequencies at which the first resonance should occur, using the measured rod velocities, are marked at the tops of figures 7 and 8. This resonance phenomenon, of course, is not predicted by the infinite cylinder theory.

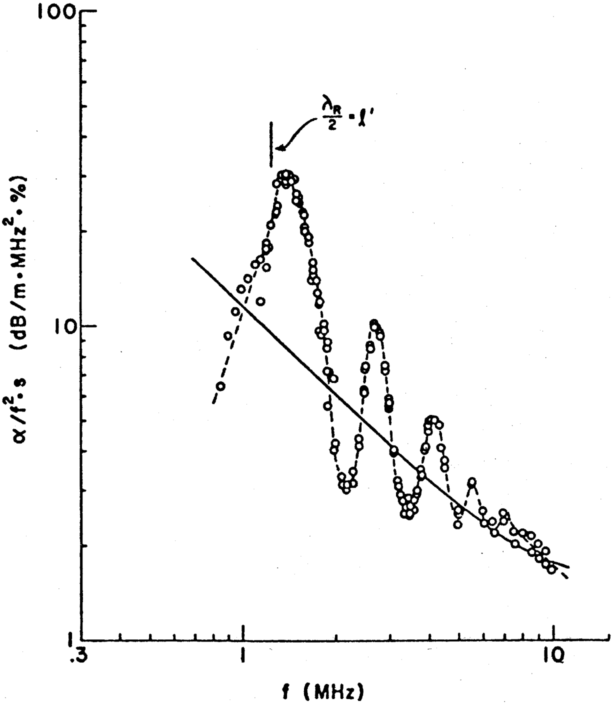

Fig 8—Experimental attenuation data for a polyester fibre slurry identical to that of Figure 7, except ℓ' = 1.66 mm. The model curve is the same as in Figure 7.

3. RAYON

Rayon is similar to nylon in that it is hygroscopic, and that water acts as a plasticiser. The velocity of the longitudinal rod wave in saturated rayon is less than in nylon, so that finite length effects are even less significant than in nylon. For the fibre radii studied ($R' > 7\mu m$), thermal effects contribute only a few percent to the attenuation. Preliminary theoretical curves indicate that attenuation is more sensitive to the value of the loss factor in rayon than in nylon. This means there are two adjustable parameters, the loss factor and Poisson's ratio (fibre modulus is found from the measured rod velocities). Loss tangent is a function of frequency but, for simplicity, the model neglects this.

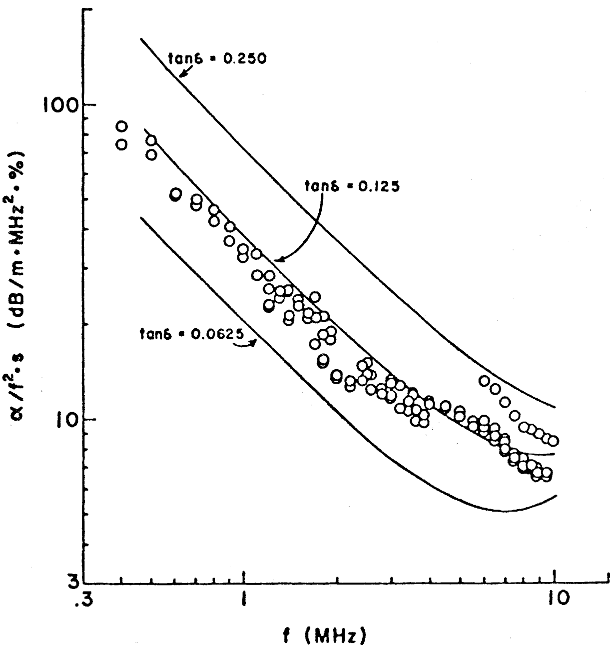

Fig 9—Experimental attenuation data for regular modulus, 2.3 mm long rayon fibres with radii from 11—15 μm. The theoretical curves have different loss tangents. The model fibre parameters are $\rho' = 1400$ kg/m^3; $c' = 1090$ m/sec; $\nu' = 0.32$; $K' = 0.15$/m°K; $Cp' = 1.5 \times 10^3$ J/kg°K; $\beta' = 3.6 \times 10^{-4}$/°K; $R' = 13 \times 10^{-6}$ m; and s = 1.25%.

Figure 9 shows the theoretical and experimental curves for normal modulus, 9.0μm radius, 2.3mm long rayon fibres. The value of Poisson's ratio is 0.32 and the loss factor has been varied to produce the different model curves. The rod longitudinal velocity was measured as 0.91 km/s. Good agreement with experiment is obtained when the values of the Poisson's ratio and loss factor are 0.32 and 0.1 respectively, but there are surely other combinations giving an equally good fit.

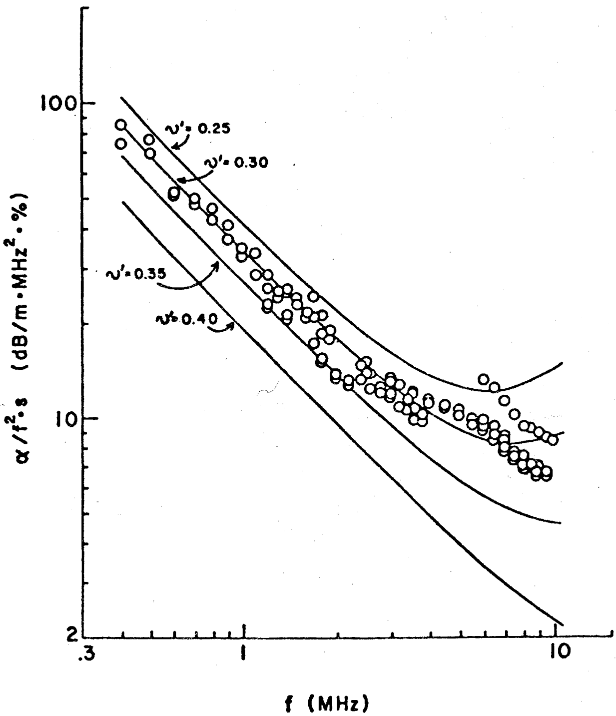

Fig 10—Experimental attenuation data for regular modulus, 2.3 mm long rayon fibres with radii from 11–15 μm. The theoretical curves have different Poisson's ratios. The model fibre parameters are $\rho' = 1400$ kg/m^3; $c' = 1090$ m/sec; $K' = 0.15$/m°K; $Cp' = 1.5 \times 10^3$ J/kg°K; $\beta' = 3.6 \times 10^{-4}$/°K; $R' = 13 \times 10^{-6}$ m; $\tan\delta = 0.1$; and $s = 1.25\%$.

Figure 10 is a set of model curves for this rayon fibre with the value of the loss factor set to 0.1 and variable Poisson's ratios. Notice this trend is the reverse of nylon (Figure 5) where increasing values of Poisson's ratio (or decreasing shear modulus) led to increasing attenuation.

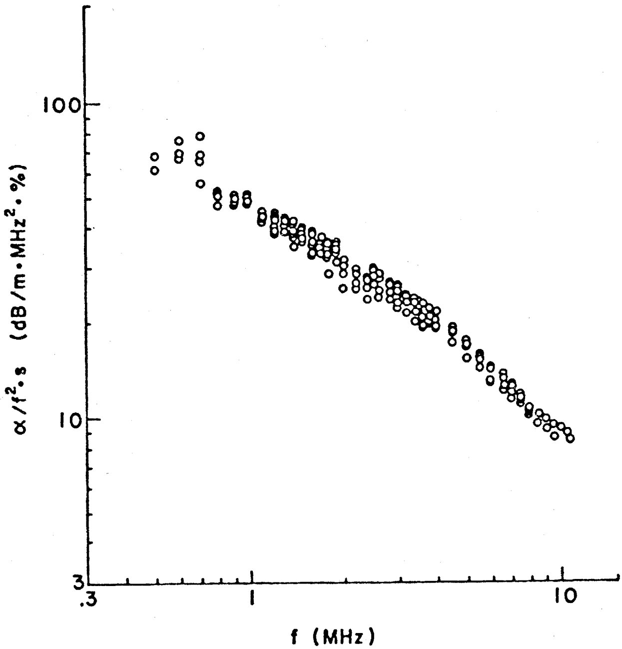

Fig 11—Experimental attenuation data for high wet modulus, 2.3 mm long rayon fibres with radii from 7 to 10 μm.

Figure 11 shows the experimental results for a 7.5μm high wet modulus rayon fibre slurry. The rod longitudinal velocity is 1.27 km/s in the saturated fibre. The level of attenuation is about the same as for the other rayon fibre, although the curve is flatter at the lower frequencies. Reasonable values of the loss factor and Poisson's ratio can be chosen to give the correct average value of attenuation, but the theory is not as successful in reproducing the shape of the curve. It is possible that the theory is less suitable for high wet-modulus rayon because it is more elastically anisotropic. Another possible explanation is that there is a visco-elastic absorption peak in this frequency regime so that the loss factor varies rapidly with frequency. This is consistent with the observations that the loss factor necessary to fit average theory to experiment is greater than in the regular rayon.

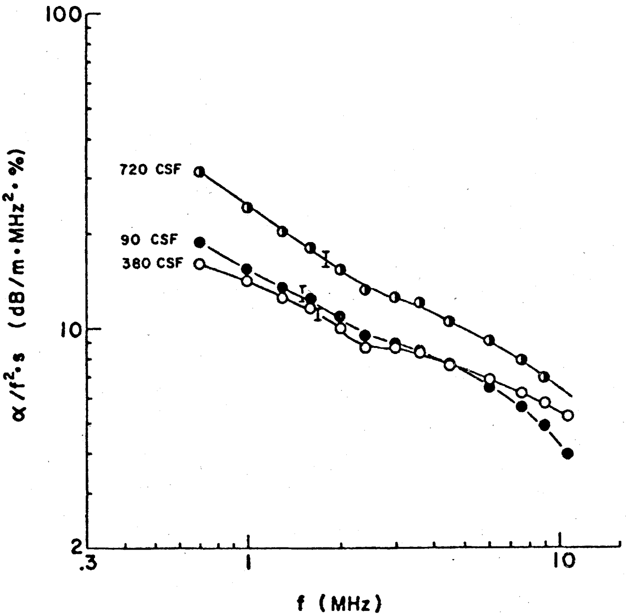

Fig 12—Average experimental attenuation data for a bleached kraft softwood pulp at freenesses of 720, 380 and 90 CSF. Each data point is the average of about 25 measurements.

4. WOOD FIBRES

Figure 12 shows the experimental data for a bleached kraft softwood pulp at different refining levels. Each data point is the average of about 25 measurements. The data are taken on pulp with consistencies from 0.48% to 2.89%. The transducer separation distance varies from 50 to 150mm. Important points to notice are the following:

1) the level of attenuation is considerably lower than that measured for rayon fibres;

2) there is a remarkably larger decrease in attenuation during the early stages of refining;

3) for highly beaten pulp the decrease wanes and reverses at the lower frequencies.

Wood fibre slurries are, of course, much more complex than synthetic fibre slurries. There are broad distributions in the shapes and sizes of the fibres, and the cross sections are not cylindrical. The mechanical and thermodynamic properties vary in a similar way and are not easily determined. Beating is not well understood in terms of its effect on the geometric, thermodynamic, and mechanical fibre properties. Nonetheless, with insight gained from the work on synthetic fibres, it is possible to conjecture as to what may be happening in this wood pulp system.

A possible explanation for the difference between rayon and wood fibres in the level of attenuation may be due to a higher degree of crystallinity in the wood fibres. This leads to a lower loss tangent and, therefore, lower attenuation. It was shown in figure 9 that rayon is quite sensitive to change in loss tangent.

There is a number of changes occurring during refining that could alter the curves. The theory predicts that a decrease in the representative radius of the fibres would lower the attenuation. However, this effect is not large enough to explain the large decrease in attenuation brought about by refining, if the radius is assumed to be initially less than about 20μm. Large particles (50 to 500μm radii) in the slurry would produce a scattering peak in the experimental frequency range. Though small in number, these particles could make a large contribution, and if refining reduced their number, it could significantly reduce attenuation.

One effect of refining could be to reduce the fibre shear modulus while keeping Young's modulus relatively constant. In the theoretical model, this corresponds to an increase in Poisson's ratio at constant rod longitudinal velocity. As shown in figures 5 and 10, changing Poisson's ratio can have a large effect on attenuation. For rayon fibres, where the velocity of the longitudinal wave in the fibre is lower than in water, increasing Poisson's ratio decreases attenuation. For nylon, where the velocity is greater than in water, the trend reverses. Wood fibres probably have a greater velocity than rayon and may be in a transition region. If the wet modulus of the wood fibres is not too much greater than that of rayon, the decrease in attenuation with refining might be due to decreasing shear modulus.

It is clear that more work needs to be done on well-characterised wood pulp systems before we have a clear understanding of ultrasound attenuation in pulp. However, the major effects have been identified. Quantitative results have been correctly predicted for synthetic fibre systems, and quantitative explanations for the observed behaviour in wood pulp systems suggests that further study is warranted.

REFERENCES

1. McFarlane, I. D., and Llewellyn, J. D., Paper 2/2, 2nd International Federation of Automatic Controls, Proc. Brussels, 1971.
2. Adams, D.J., 3rd International Federation of Automatic Control Proc. Brussels, 1976. p. 187.
   Adams, D.J., Ultrasonic Transmission Through Paper Fibre Suspensions. Ph.D. Thesis. University of London, 1975.
3. Lord Rayleigh, Theory of Sound,. Vol. II, Dover, 1945.
4. Allegra, J.R. and Hawley, S.A., J. Acoust. Soc. Am., 1972 **51**(5,Part 2), p.1545
5. Biot, M.A., J. Acoust. Soc. Am. 1956, **28**(2), p.168 and 1962, **33**(4), p.1482
6. Epstein, P.S., and Carhart, R.R., J. Acoust. Soc. Am., 1953, **25**(3), p.553

APPENDIX

Outline of the theoretical development

List of symbols

r,θ,z	Cylindrical co-ordinates aligned with the fibre	a_{cc}'	$R'k_{cc}'$
t	Time	k_t	$(i\omega\rho C_p/K)^{1/2}$
R'	Cylinder radius	a_t	$R'k_t$
T	Temperature	k_{tc}	$(k_t^2-k_{cs}^2)^{1/2}$
fr	Solid volume fraction	a_{tc}	$R'k_{tc}$
ω	Angular frequency	k_s	$(i\omega\rho/\eta)^{1/2}$
e	Angle between the plane of the fibre and the incoming radiation	a_s	$R'k_s$
$\vec{A}$	Transverse wave vector potential	k_s'	$\omega(\rho'/\mu')^{1/2}$
φ	Comparison wave potential	a_s'	$R'k_s'$
ψ,ξ	Scalar potentials for transverse wave	k_{sc}	$(k_s^2-k_{cs}^2)^{1/2}$
c	Compressional wave velocity	k_{sc}'	$(k_s'^2-k_{cs}^2)^{1/2}$
l'	Fibre length	a_{sc}	$R'k_{sc}$
ρ	Density	b_c	$-\beta T\omega^2/C_p$
η	Viscosity	C_{12}	$c^2+4i\omega\eta/3\rho$
ν'	Solid Poisson's ratio	C_{12}'	$c'^2-4\mu'/3\rho$
μ'	Solid shear Lamé constant	γ	$1+\beta^2Tc^2/C_p$
K	Heat conductivity coefficient	b_t	

C_p	Heat capacity	b_t'	
β	Thermal expansivity	J_n	n′th order Bessel of first kind
$\tan \delta$	Solid loss tangent	$H_n^{(1)}$	n′th order Hankel function of first kind
k_c	ω/c	J_n'	1st derivative of J_n
a_c	R'/k_c	J_n''	2nd derivative of J_n
k_c'	$\omega/c'(1-i\tan \delta)^{1/2}$	$H_n^{(1)\prime}$	1st derivative of $H_n^{(1)}$
a_c'	$R'k_c$	$H_n^{(1)\prime\prime}$	2nd derivative of $H_n^{(1)}$
k_{cs}	$k_c \sin e$	B_n, C_n, D_n, E_n	Undetermined coefficients
a_{cs}	$R'k_{cs}$	s	consistency
k_{cc}	$k_c \cos e$	f	frequency
a_{cc}	$R'k_{cc}$	$\vec{V}$	Velocity vector
k_{cc}'	$(k_c'^2-k_{cs}^2)$		

Primed symbols refer to the solid and unprimed to the liquid. When primed symbols are unlisted they have definitions analogous to the unprimed symbols.

The problem is to find a solution for temperature and velocity to the continuity equation, the equations of motion, and the energy conservation equation, which meets the required boundary conditions at the cylinder-fluid interface and is a plane wave at an angle e to the axis of the cylinder far away from it. It is shown by Epstein and Carhart[6] and Allegra and Hawley[4] that the governing equations can be linearised for small motions and expressed in teerms of potentials, A and φ. The governing equations are satisfied if equations (1) - (4) are obeyed and the velocity and temperature are related to the potentials as in equations (5) and (6).

$$\vec{\nabla}\cdot\vec{A} = 0 \tag{1}$$

$$\nabla^2\phi_c = -k_c{}^2\phi_c \tag{2}$$

$$\nabla^2\phi_t = -k_t{}^2\phi_t \tag{3}$$

$$\vec{\nabla}\mathrm{x}\vec{\nabla}\mathrm{x}\vec{A} = -k_s{}^2\vec{A} \tag{4}$$

$$\vec{V} = -\vec{\nabla}\phi_c - \vec{\nabla}\phi_t + \vec{\nabla}\mathrm{x}\vec{A} \tag{5}$$

$$T = b_c\phi_c + b_t\phi_t \tag{6}$$

Equations (1) - (6) apply in the solid as well as in the fluid. Here the corresponding symbols will be denoted by a prime.

When the incoming plane wave is expanded in terms of Bessel functions, it becomes

$$\varphi_o = [J_o(k_{cc}r) + 2\sum_{n=1}^{\infty} i^n\cos n\theta\ J_n(k_{cc}r)]e^{i(k_{cs}z-\omega t)} \tag{7}$$

Solutions to equations (2) and (3) can be expanded similarly with undetermined coefficients. The results are:

$$\varphi = \varphi_o + \varphi_r + \varphi_t, \tag{8}$$

$$\text{and, } \varphi' = \varphi_c' + \varphi_t' \tag{9}$$

Where

$$\varphi_r = B_o H_o^{(1)}(k_{cc} r) + 2 \sum_{n=1}^{\infty} B_n i^n \cos n\theta \, H_n^{(1)}(k_{cc} r)\, e^{i(k_{cs} z - \omega t)}, \tag{10}$$

$$\varphi_t = C_o H_o^{(1)}(k_{tc} r) + 2 \sum_{n=1}^{\infty} C_n i^n \cos n\theta \, H_n^{(1)}(k_{tc} r)\, e^{i(k_{cs} z - \omega t)}, \tag{11}$$

$$\varphi_{c'} = B'_o J_o(k'_{cc} r) + 2 \sum_{n=1}^{\infty} B'_n i^n \cos n\theta \, J_n(k'_{cc} r)\, e^{i(k_{cs} z - \omega t)}, \tag{12}$$

$$\varphi_{t'} = C'_o J_o(k'_{tc} r) + 2 \sum_{n=1}^{\infty} C'_n i^n \cos n\theta \, J_n(k'_{tc} r)\, e^{i(k_{cs} z - \omega t)}, \tag{13}$$

In the above, solutions which have the same time and z dependence as the incoming radiation (i.e., $e^{i(k_{cs} - \omega t)}$) are being sought.

The boundary conditions at $r = R'$ are

a) $V_r = V_r'$	b) $V_\theta = V_\theta'$	c) $V_z = V_z'$
d) $T = T'$	e) $KT,r = k'T',r$	f) $t_{rr} = t_{rr}'$
g) $t_{r\theta} = t_{r\theta}'$	h) $t_{rz} = t_{rz}'$	

To meet these eight boundary conditions, two linearly independent solutions to equations (1) and (4) are needed. It can be shown that A_1 and A_2 are solutions to equations (1) and (4) when

$$A_1 = \vec{\nabla} \times \Psi\hat{k} \quad \text{and} \quad A_2 = \vec{\nabla} \times \vec{\nabla} \times \xi\hat{k},$$

$$\text{if} \quad \nabla^2\Psi = -k_s{}^2\Psi \quad \text{and} \quad \nabla^2\xi = -k_s{}^2\xi$$

Now the ξ's and ψ's are expanded in Bessel and cosine functions.

$$k_s{}^2\xi = [D_oH_o{}^{(1)}(k_{sc}r) + 2\sum_{n=1}^{\infty} D_n i^n \frac{d\cos n\theta}{d\theta} H_n{}^{(1)}(k_{sc}r)]e^{i(k_{cs}z-\omega t)} \quad (14)$$

$$ik_{cs}\Psi = [E_oH_o{}^{(1)}(k_{sc}r) + 2\sum_{n=1}^{\infty} E_n i^n \frac{d\cos n\theta}{d\theta} H_n{}^{(1)}(k_{sc})]e^{i(k_{cs}z-\omega t)} \quad (15)$$

$$k_s{}'\xi' = [D_o{}'J_o(k_{sc}{}'r) + 2\sum_{n=1}^{\infty} D_n{}' i^n \frac{d\cos n\theta}{d\theta} J_n(k_{sc}{}'r)]e^{i(k_{cs}z-\omega t)} \quad (16)$$

$$ik_{cs}\Psi' = [E_o{}'J_o(k_{sc}{}'r) + 2\sum_{n=1}^{\infty} E_n{}' i^n \frac{d\cos n\theta}{d\theta} J_n(k_{sc}{}'r)]e^{i(k_{cs}z-\omega t)} \quad (17)$$

When the velocities and temperature are expressed in terms of the potentials by equations (5) and (6), the eight boundary conditions can be expressed in terms of eight sets of undetermined coefficients. Because of the orthogonality of the $\cos n\theta$'s, the boundary conditions must hold for each order of coefficients. This results in eight equations and eight unknowns for each order, n, of the coefficients. The resulting equations are

(a) $$a_{cc}J_n{}'(a_{cc}) + B_na_{cc}H_n{}^{(1)\prime}(a_{cc}) + C_na_{tc}H_n{}^{(1)\prime}(a_{tc}) - E_na_{sc}H_n{}^{(1)\prime}(a_{sc}) + n^2D_nH_n{}^{(1)}(a_{sc}) = -i\omega[B_n{}'a_{cc}{}'J_n{}'(a_{cc}{}') + C_n{}'a_{tc}{}'J_n{}'(a_{tc}{}') - E_n{}'a_{sc}{}'J_n{}'(a_{sc}{}') + n^2D_n{}'J_n(a_{sc}{}')], \quad (18)$$

(b) $$J_n(a_{cc}) + B_nH_n{}^{(1)}(a_{cc}) + C_nH_n{}^{(1)}(a_{tc}) - E_nH_n{}^{(1)}(a_{sc}) + D_na_{sc}H_n{}^{(1)\prime}(a_{sc}) = -i\omega[B_n{}'J_n(a_{cc}{}') + C_n{}'J_n(a_{tc}{}') - E_n{}'J_n(a_{sc}{}') + D_n{}'a_{sc}{}'J_n{}'(a_{sc}{}')], \quad (19)$$

(c) $$a_{cs}{}^2J_n(a_{cc}) + a_{cs}{}^2B_nH_n{}^{(1)}(a_{cc}) + a_{cs}{}^2C_nH_n{}^{(1)}(a_{tc}) + a_{sc}{}^2E_nH_n{}^{(1)}(a_{cc}) = -i\omega[a_{cs}{}^2B_n{}'J_n(a_{cc}{}') + a_{cs}{}^2C_n{}'J_n(a_{tc}{}') + a_{sc}{}'^2E_n{}'J_n(a_{sc}{}')], \quad (20)$$

(d) $$b_c[J_n(a_{cc}) + B_nH_n{}^{(1)}(a_{cc})] + b_tC_nH_n{}^{(1)}(a_{tc}) = -i\omega[b_c{}'B_n{}'J_n(a_{cc}{}') + b_t{}'C_n{}'J_n(a_{tc}{}')], \quad (21)$$

(e) $$K[a_{cc}b_c(J_n{}'(a_{cc}) + B_nH_n{}^{(1)\prime}(a_{cc})) + C_nb_ta_{tc}H_n{}^{(1)\prime}(a_{tc})] = -i\omega K'[B_n{}'b_c{}'a_{cc}{}'J_n{}'(a_{cc}{}') + C_n{}'b_t{}'a_{tc}{}'J_n{}'(a_{tc}{}')], \quad (22)$$

(f) $\eta\big([(a_s{}^2-2a_c{}^2)J_n(a_{cc}) - 2a_{cc}{}^2J_n''(a_{cc})] + B_n[(a_s{}^2 - 2a_c{}^2)H_n(a_{cc})$
$-2a_{cc}{}^2H_n{}^{(1)''}(a_{cc})] + C_n[(a_s{}^2-2a_t{}^2)H_n{}^{(1)}(a_{tc}) - 2a_{tc}{}^2H_n{}^{(1)''}(a_{tc})] +$
$2E_na_{sc}{}^2H_n{}^{(1)''}(a_{sc}) + 2D_nn^2[H_n{}^{(1)}(a_{sc}) - a_{sc}H_n{}^{(1)'}(a_{sc})]\big) =$
$B_n'[(\omega^2\rho'R'^2 - 2\mu'a_c'^2)J_n(a_{cc}') - 2\mu'a_{cc}'^2J_n''(a_{cc}')] +$
$C_n[(\omega^2\rho'R'^2 - 2\mu'a_t'^2)J_n(a_{tc}') - 2\mu'a_{tc}'^2J_n''(a_{tc}')] +$
$2\mu'E_n'a_{sc}'^2J_n(a_{sc}') + 2\mu'D_n'n^2[J_n(a_{sc}') - a_{sc}'J_n(a_{sc}')],$ (23)

(g) $\eta\big(a_{cc}J_n'(a_{cc}) - J_n(a_{cc}) + B_n[a_{cc}H_n{}^{(1)'}(a_{cc}) - H_n{}^{(1)}(a_{cc})] +$
$C_n\ [a_{tc}H_n{}^{(1)}(a_{tc}) - H_n{}^{(1)}(a_{tc})] + \frac{D_n}{2}\ [n^2H_n{}^{(1)}(a_{sc}) - a_{sc}H_n{}^{(1)'}(a_{sc}) +$
$a_{sc}{}^2H_n{}^{(1)''}(a_{sc})] + E_n\ [H_n{}^{(1)}(a_{sc}) - a_{sc}H_n{}^{(1)'}(a_{sc})]\big) =$
$\mu'\big(B_n'[a_{cc}'J_n'(a_{cc}') - J_n(a_{cc}')] + C_n'[a_{tc}'J_n'(a_{tc}') - J_n(a_{tc}')] +$
$\frac{D_n'}{2}\ [n^2J_n(a_{sc}') - a_{sc}'J_n'(a_{sc}') + a_{sc}'^2\ J_n''(a_{sc}')] + E_n'[J_n(a_{sc}') -$
$a_{sc}'J_n'(a_{sc}')]\big)$, and (24)

(h) $2\eta a_{cc}a_{cs}[J_n'(a_{cc}) + B_nH_n{}^{(1)'}(a_{cc})] + 2\eta a_{tc}a_{cs}C_nH_n{}^{(1)'}(a_{tc}) +$
$\eta E_nH_n'(a_{sc})[a_{sc}{}^2 - a_{cs}{}^2]a_{sc}/a_{cs} + \eta D_nn^2a_{cs}H_n{}^{(1)}(a_{sc}) = 2\mu'a_{cc}'a_{cs}$
$B_n'J_n'(a_{cc}') + 2\mu'a_{tc}'C_n'J_n'(a_{tc}')a_{cs} + \mu'D_n'n^2a_{cs}J_n(a_{sc}') +$
$\mu'E_n'J_n'(a_{sc}')a_{sc}'[a_{sc}'^2 - a_{cs}{}^2]/a_{cs}.$ (25)

These eight simultaneous equations are solved numerically for $n = 0,1$, and 2. When k_cR' and $k_c'R'$ are less than one, the series converges rapidly, and the first three terms provide an excellent approximation to the solution.

A rather lengthy calculation, modeled after the Epstein and Carhart[6] spherical development, expresses the attenuation coefficient, a, for fibres at an angle e to the radiation as

$$a = \frac{-4fr}{\pi R'^2 k_c} \left[\mathrm{Real}(B_o) + \sum_{n=1}^{\infty} 2\mathrm{Real}(B_n)\right]. \tag{26}$$

The B_n's are function's of e; therefore to find a for a random orientation the simultaneous equations must be evaluated at a series of e's between 0° and 90° and averaged. This is done by integrating numerically the following expression:

$$a_{random} \simeq \frac{-4fr}{\pi R'^2 k_c} \int_0^{\pi/2} \mathrm{Real}[B_o + 2(B_1 + B_2)] \cos e \, de. \tag{27}$$

This process can be repeated at different frequencies, and the attenuation vs. frequency relationship predicted from the physical propertie: of the slurry.

Transcription of Discussion

Discussion

Discussion following paper of Dr. G.A. Baum

Dr. D. Wahren, IPC: Chairman

It is very interesting to see such precise work being done. I am especially interested to see that it doesn't affect the results whether or not the fibres form a coherent network. Have you any comment to make on this?

Dr. G.A. Baum, IPC

Our model assumes the fibres to be all independent. It is possible that a coherent network exists, which if it did, would represent a perturbation on the results.

Dr. D. Wahren

Your method of normalisation, which involves dividing by consistency at constant freeness, implies that networks are not very important.

Dr. G.A. Baum

From the observation that the quantity a/f^2 is linear with consistency, one would certainly reach that conclusion.

Dr. D.W. Clayton, Paprican

Earlier you showed some results you obtained when you increased the radii of some nylon fibres from 15 to 111 microns. This seems like rather a large jump. Have you any results for intermediate radii?

Dr. G.A. Baum

No, we did not obtain results for intermediate values. One of the useful properties of the model is that it allows us to change only one variable at a time. As the fibre diameter is increased then scattering phenomena become important at high frequencies. Further increases of diameter extend downwards the frequency at which scattering becomes important.

Prof. R. Kerekes, Paprican

I would like to say something here, which might help you with your hypotheses. At Paprican we recently measured fibre flexibility after beating in a PFI mill over the freeness range from 720 to 300 CSF, similar therefore to the range you investigated. The measured increase in fibre flexibility is approximately twofold. As you know, the flexibility reflects a combination of the elastic modulus and the geometric configuration of the fibres, and may thus be an important parameter in your studies.

Dr. G.A. Baum

Thank you. We are aware of your work and have tried to take your results into account when explaining the effects with wood pulp fibres.

Prof. K.I. Ebeling, Helsinki University of Technology, Finland

All your analysis is based on the rigid rod model. Is it possible that some of the discrepancies might be removed by considering a porous solid model? The porous nature would obviously be derived from the presence of the lumen and the fibrillar structure of the cell wall.

Dr. G.A. Baum

In our work we have tried to keep the model as simple as possible. Adams was forced to consider a porous model because he found that the ultrasonic velocity depended on frequency, which can′t be accounted for by the isolated segment model. The Biot model is very complicated and incorporates many parameters. We have been successful in explaining our measurements on synthetic fibre systems and plan to concentrate on well-characterised fibre suspensions at present, while retaining the simple model. It is quite possible that the irregular shape and anisotropic nature of wood fibres affects the attenuation.

Dr. C.C. Habeger, IPC

A porous model would be expected to display some form of percolation phenomenon, so that the attenuation could not be expected to be linear with respect to consistency. Since we find this linear relationship between these two quantities, we see no need to complicate the model at present.

Dr. M.B. Lyne, Paprican

In the samples where the pulp was beaten did you take any steps to separate out the fibres, and do the fines have any effect on the attenuation?

Dr. C.C. Habeger

We did not separate out the fines. The model predicts that the absorption per unit mass decreases with radius at these frequencies, so that the part of the total mass present as fines should not contribute significantly to the total absorption.

Mr. B. Radvan, Wiggins Teape, UK

It is curious that there should be no effect of any network structure on the attenuation. It is just possible that this is because the wavelengths you are using (of the order of fractions of a millimetre) are too short to see the flocs. You have observed the resonance between the wave and the ends of the free, rigid cylinders, so if you were to increase the wavelength to the order of 10 mm or so then you might observe the effect of the floc structure.

Dr. C.C. Habeger.

That is perfectly possible, but, quite honestly, I would expect the effect to be small.

Prof. T. Helle, The University of Trondheim, Norway.

If you used dried pulps, then the results shown in figure 12 are exactly as I would expect. At the commencement of beating, the flat, ribbon-like fibres become more flexible, but as it continues balloons start to develop because of the imbided water, and the fibres become stiffer. This would appear to account for the results you obtained.

Dr. G.A. Baum

The model predicts that the attenuation should increase as the fibre flexibility, given by 1/EI, increases.

Mr. A. de Ruvo, STFI, Sweden

The damping you refer to is the mechanical damping of the material under study, and is at least partly associated with plasticisation. Could you envisage performing your measurements on a mechanical pulp at elevated temperatures around 80 - 90°C which we believe to be the glass transition temperature of lignin? Could such an experiment be a good way of observing the glass transition?

Dr. C.C. Habeger

The theory, and I think the experimental results, shows that the absorption is quite sensitive to relaxation phenomena in the fibre. If there was a relaxation peak in the lignin absorption curve at the appropriate temperature and frequency, then the attenuation ought to be dependent upon the amount of lignin present.

Mr. A. de Ruvo

Then it might also be possible to check the influence of the chemical environment, for example the effect of pH.